American Journal of Mechanical Engineering and Automation
2016; 3(2): 11-21
http://www.openscienceonline.com/journal/ajmea
ISSN: 2381-6198 (Print); ISSN: 2381-6201 (Online)

Open Science

Effects of Kind of Fluid on the Flutter Speed of Turbine Blades

Mohammad Amin Rashidifar[1], Ali Amin Rashidifar[2], Abdullah Abertavi[2]

[1]Department of Mechanical Engineering, Islamic Azad University, Shadegan Branch, Shadegan, Iran

[2]Department of Electrical and Computer Science, Islamic Azad University, Shadegan Branch, Shadegan, Iran

Email address

rashidifar_58@yahoo.com (M. A. Rashidifar), shadegan_950@yahoo.com (A. A. Rashidifar), abertavi_195@yahoo.com (A. Abertavi)

To cite this article

Mohammad Amin Rashidifar, Ali Amin Rashidifar, Abdullah Abertavi. Effects of Kind of Fluid on the Flutter Speed of Turbine Blades. *American Journal of Mechanical Engineering and Automation.* Vol. 3, No. 2, 2016, pp. 11-21.

Received: March 20, 2016; **Accepted**: March 31, 2016; **Published**: June 24, 2016

Abstract

In this research paper, a row of blades which consist of a tuned disk and certain number of blades and will be examined. Curved blades that cross a series of free moments of inertia due to bending by cantilevered beams are modeled. Regarding that the disk being tuned, the whole structural and fluid system analysis is focused on a blade and the current around it. Aerodynamic forces during stable and unstable motion in several steps are calculated using ANSYS/ FLOTRAN CFD software and then the real and unreal forces fluid are obtained. On the other hand, the equation of motion in Timoshenko beam is obtained and to determine the system natural frequencies and modes, outside forces are zero and modal analysis while the bending and torsion movements of exposure mode have been done is carried out. By using semi inertia and semi damping and semi elastic of fluid's elements in inertia and damping and stiffness matrix we can have an eigenvalue equation that solved by using state space method. In this case we can obtain flutter speed of turbine. Then comparison between steam and gas effect as flow on flutter speed were studied.

Keywords

Blade, Aerodynamics, Flutter, ANSYS CFD, Timoshenko Beam

1. Introduction

Aeroelasticity is a science concerned with mutual interactions among structural (inertial and elastic) and aerodynamic characteristics of a structure immersed in a flowing fluid. It consists of three main subjects; Structure, Dynamics, and Aerodynamics. Aeroelasticity study of turbomachinery can be roughly classified in two categories: self-excited vibration and forced response. Self-excited vibration of a lifting surface in a gas stream results from a continuous interaction between aerodynamics and structural mechanics, in such a manner that the vibrating structure begins to extract energy from the flowing fluid, when the structure will experience an oscillation. Flutter is a kind of self-excited vibration which is dynamically unstable and is a self-sustained divergent oscillation. Flutter can limit the output load of turbomachineries such as gas turbines. Self-excited aeroleastic vibrations also include near flutter operation which may cause high or low cycle fatigue. In some blades that may operate close to the resonance speed. For this reason flutter analysis may be provided to give the desired life. Otherwise, the blades are susceptible for failures (Rao and Saldanha). The major concern of this paper is all types of self-excited aeroelastic vibrations encountered in gas and steam turbine blades.

One of the earlier studies considering airfoil geometries was a research done by Whitehead (1962) on ideal flows around straight airfoils which have rigid translational and torsional oscillations. By 1970, isolated airfoil theory of wings was conventionally used considering thin and straight airfoil for flutter prediction.

In compressor and turbine airfoils, a proper camber is considered in design with the intent of having pressure and suction side. This factor increases radius of gyration and also rotary inertia and shear deformation. The aerodynamic effects of airfoil camber have already been discussed, however with less attention to structural behavior. Atassi and

Akai (1980) developed a method for studying airfoils having thickness and camber and concluded that airfoil geometry have considerable effects on unsteady aerodynamic loadings.

FEM approaches were then used in plate or solid models of structures by Moffatt and Hi (2003). Plate and beam models do not have rotary inertia and shear deformation capabilities. Solid models restricted to quasi-3D flutter analysis and FEM approaches, so Timoshenko beam theory is presented, Thereby blades can be analyzed analytically and by FEM methods regarding rotary inertia and shear deformation. Therefore, some supplementary concepts are introduced considering this aspect.

By introducing Timoshenko beam theory, the effects of camber on flutter suppression can be investigated considering differences in five aspects: moment of inertia, aerodynamic loading, bending/torsion coupling, rotary inertia and shear deformation. In this research, flutter properties of cambered airfoils based on steam and gas as fluid were compared.

2. Deriving the Equation of Motion by using Timoshenko Beam Theory

If in the study of the dynamic behavior of beam, rotary inertia and shear deformation are also taken into account, then these kinds of beams are modeled as Timoshenko beams.

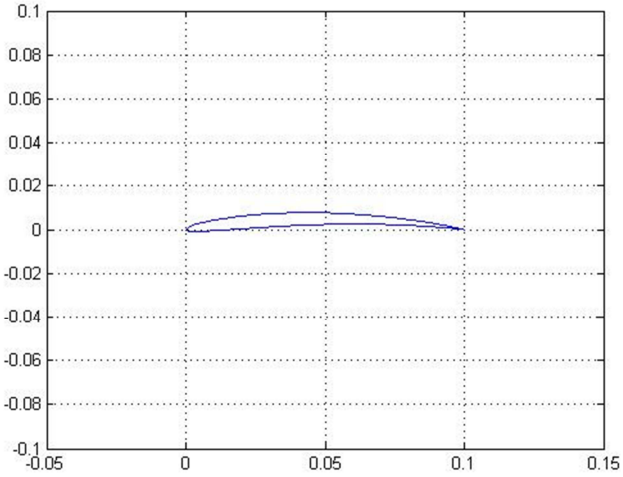

Figure 1. *The plot of camber airfoil.*

The governing equation of motion of the beam in generalized coordinate (q) can be obtained based on Hamilton principle. After simplification, the equation set of motion is established as:

$$\begin{cases} m\ddot{w} - m\bar{x}\ddot{\theta} - k'AGw'' + k'AG\psi' = F(x,t) \\ \rho_s I\ddot{\psi} - IE\psi'' - k'AGw' + k'AG\psi = 0 \\ mr^2\ddot{\theta} - m\bar{x}\ddot{w} - GJ\theta'' = M(x,t) \end{cases} \quad (1)$$

Noting the fact that the blades of compressors are usually fixed at the roots, overhung boundary conditions must be satisfied.

In eq.1, bending and torsion are coupled to each other. Before determining the final equation of the body in coupled form, the external forces must be set to zero and the above relations are applied in decoupled form for determination of natural frequencies and their relating modes. The term that contains $\bar{x}$ is omitted by shifting the x coordinate to the center of the airfoil.

2.1. Establishment of the Generalized Equation in Dynamic and Force Coupling Form

In this equation, the bending and torsion and on the other hand, force and the relations of motion are coupled. In other words, there is force coupling in addition to dynamic coupling.

Based on Rayleigh-Ritz method, w , ψ and θ are the result of their corresponding normal modes superposition. Considering one mode

$$T = q = e^{i\omega_j t},\ w = \phi_j(y)(q_h)_j \quad (2)$$

$$\psi = \psi_j(y)(q_h)_j,\ \theta = \theta_j(y)(q_\theta)_j.$$

Yield a set of equations in the form of

$$\begin{bmatrix} m_h & -B\bar{x} \\ -B\bar{x} & m_\theta \end{bmatrix}\begin{bmatrix} \ddot{q}_h \\ \ddot{q}_\theta \end{bmatrix} + \begin{bmatrix} \omega_h^2 m_h & 0 \\ 0 & \omega_\theta^2 m_\theta \end{bmatrix}\begin{bmatrix} q_h \\ q_\theta \end{bmatrix} = \begin{Bmatrix} F_G \\ M_G \end{Bmatrix}$$

$$m_h = \int_0^l m\phi_i^2 \frac{dy}{l} + \int_0^l mr_h^2\psi_i^2 \frac{dy}{l}$$

$$m_\theta = \int_0^l \rho_s J\theta_i^2 \frac{dy}{l} + \int_0^l mr_\theta^2\theta_i^2 \frac{dy}{l}$$

$$F_G = \int_0^l F\phi_i \frac{dy}{l} + \int_0^l M_\psi\psi_i \frac{dy}{l}$$

$$M_G = \int_0^l M_\theta\theta_i \frac{dy}{l} \quad (3)$$

$$B = \int_0^l \rho_s A\phi_i\,\theta_i \frac{dy}{l}$$

m_h ، m_θ ، F_G ، M_G and B are the generalized mass in bending and torsion, the generalized force in bending and torsion and coupling term respectively. Having the mode shape from the previous steps, these parameters can be achieved.

In order to simplify the relations and expressing clearly and generally, the mode shape of the lateral, bending and pitching vibrations are normalized. Furthermore, as the thickness and the mass along the span are assumed constant in the current report, this equation is further simplified by taking m out of the integral and dividing the two sides by m. Moreover, assuming a light damping of the structure, the damping is also considered based on the conventional methods.

Consequently, the mode shapes are normalized without considering inertial factors.

$$m_h = m\int_0^l (\phi_i^2 + r_h^2\psi_i^2)\frac{dy}{l}$$

$$\int_0^l (\phi_i^2 + r_h^2\psi_i^2)\frac{dy}{l} = \phi_{norm} + \psi_{norm} = 1$$

$$m_\theta = m\int_0^l r_\theta^2\,\theta_i^2\,\frac{dy}{l} \quad \& \quad \int_0^l \theta_i^2\,\frac{dy}{l} = 1$$

The equation set is therefore reduced t

$$\begin{bmatrix} 1 & -B\bar{x} \\ -B\bar{x} & r_\theta^2 \end{bmatrix}\begin{bmatrix} \ddot{q}_h \\ \ddot{q}_\theta \end{bmatrix} + \begin{bmatrix} 2\zeta_s\omega_h & 0 \\ 0 & 2r_\theta^2\zeta_s\omega_\theta \end{bmatrix}\begin{bmatrix} \dot{q}_h \\ \dot{q}_\theta \end{bmatrix} + \begin{bmatrix} \omega_h^2 & 0 \\ 0 & r_\theta^2\omega_\theta^2 \end{bmatrix}\begin{bmatrix} q_h \\ q_\theta \end{bmatrix} = \begin{Bmatrix} \frac{F_G}{m} \\ \frac{M_G}{m} \end{Bmatrix} \tag{4}$$

Which are the generalized equation in dynamical and force coupling form. In addition, r_θ is the radius of gyration with respect to the elastic axis. Consequently, the dynamical and force coupled equation can be solved. However, the natural frequencies of bending and torsion and the relevant modes must be computed before solution. Methods for computation of these parameters will be described in the next section.

2.2. Calculating Bending Natural Frequencies and the Relevant Mode Shapes

In this case, in order to reduce the parameters, and also for possibility of converting the results to the desired dimensions, the quantities of eq. 1 are non-dimensionalized.

The first and second relationships of eq.1 are non-dimensionalized by dividing them by IE/l^2 and IE/l^6 respectively and some manipulations. Finally, the following set of equation is developed. (The dimensionless quantities are denoted by ~ over them.)

$$\begin{cases} \tilde{\rho}_s\tilde{A}\ddot{\tilde{w}} - k'\tilde{A}\tilde{G}\tilde{w}'' + k'\tilde{A}\tilde{G}\tilde{\psi}' = 0 \\ \tilde{\rho}_s\tilde{I}\ddot{\tilde{\psi}} - \tilde{\psi}'' - k'\tilde{A}\tilde{G}\tilde{w}' + k'\tilde{A}\tilde{G}\psi = 0 \\ \tilde{\rho}_s\tilde{A}\tilde{r}^2\ddot{\tilde{\theta}} - \tilde{G}\tilde{J}\tilde{\theta}'' = 0 \end{cases} \tag{5}$$

For determining the natural frequencies of bending, the decoupled equation is solved by separation of variable methods. A method was introduced by Han et al (1999) for modal analysis of Timoshenko beams. Here, the same procedure is applied for calculation of bending wave numbers (a, b) and the consecutive natural frequency and mode shape.

2.3. Calculating Pitching Natural Frequencies and the Relevant Mode Shapes

In order to find the pitching natural frequency, the third relation of eq. 1 is simplified to the following relation by separation of variable technique.

$$\rho Q\ddot{T} - GQ''T = 0$$

$$c = \sqrt{\frac{G}{\rho}} \quad \rightarrow \quad c^2 = \frac{Q''}{Q} = \frac{\ddot{T}}{T} = \omega^2 \tag{6}$$

Considering the boundary conditions of cantilever beams, the natural frequencies and the relevant mode shapes can be obtained conveniently.

$$\omega_i = \frac{(n+1/2)\pi c}{l} \qquad n = 0,1,2,3,..... \tag{7}$$

$$\theta_i = \theta_{peak}\sin(\frac{(n+1/2)\pi}{l}y)$$

2.4. Calculation of Aerodynamic Forces

In this report, aerodynamic analysis is performed by taking ANSYS/CFD/ FLOTRAN into account. ANSYS is a multiphysics product and one of its features is CFD solution of fluid systems by FEM approaches. FLOTRAN has a subset named ALE[1] that can analyze the interaction behavior of structures and fluids. ALE a conventional term for systems that includes moving boundaries between structures and fluids. Utilization of ALE can contribute significantly towards incorporating this capability in a fully-coupled aeroelastic analysis of blades by ANSYS which will be a significant improvement in aeroelasticity.

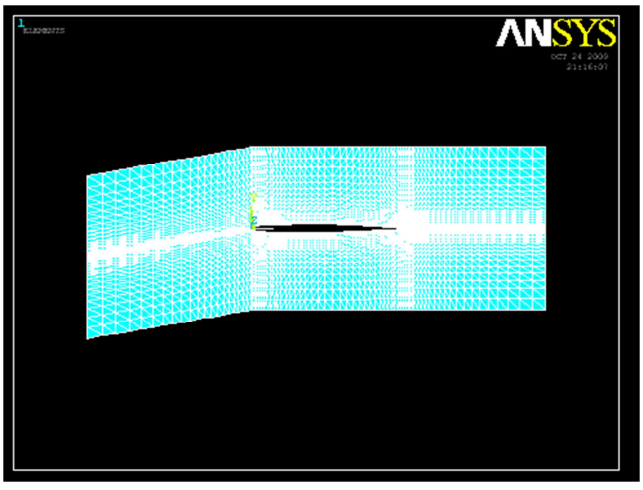

Figure 2. *2D Mapped meshing of the aerodynamic space around a typical blade.*

In aerodynamic analysis of blades, the coordinates of airfoil surface is defined at the first step. After that, the grids

1 Arbitrary Lagrangian-Eulerian method

are constructed by FLUID141 elements. Mapped meshes are used in order to have symmetrical area and the ability to apply periodic boundaries which will be described later. In order to have finer grids around leading and trailing edges, a deliberate pattern of line division is devised. The spanwise lines and inlet and exit passages are divided proportionally, so that finer meshes are placed around the leading and trailing edges as shown in Fig. 1.

The boundaries of the fluid consist of periodic boundaries, the blade surfaces, inlet and exit of the fluid. The periodic boundaries retain the circumferential nature of the problem. Herein, zero interblade phase angle is considered for periodic boundaries. If an interblade phase angle other than zero is considered, the circumferential dimension of the domain in Fig. 1 must be stretched $2\pi h/\sigma$ further. h and σ denote blade pitch and interblade phase angle, respectively. There are two methods for imposing these kinds of boundary conditions; considering two adjacent blades as periodic boundaries or considering the middle of two adjacent paths around the blade as periodic boundaries. In this report, the second method is used, and the periodic boundaries are applied at both sides of airfoils in one pitch space, so that the space between each blade and its corresponding periodic boundaries is equal to $h/2$.

At the inlet, Mach number and the angle of attack are known. If just the inlet Mach number is given, the output pressure is varied until the inlet Mach number satisfies the requirement. For preventing reflection of the entering and exiting waves (specially in supersonic flows), these boundary conditions must be imposed at a distance far from the airfoil that minimizes the influences of these reflections. In this schedule, this boundary is taken at one chord length far from the leading or trailing edges.

The most significant part of these boundary conditions is determining the condition of the border between the fluid and the structure. As stated before, in the current analysis, ALE is used for imposing these conditions. This is done in time domain by time stepping approach. At first, an adequate reduced frequency is assumed as the vibration frequency of the blade. The time wave corresponding to this frequency is then divided to small time steps (each cycle about 100 divisions) and for each moment, the horizontal and vertical coordinate of the blade is given to the program and the condition of the border between the fluid and the structure is therefore represented as *Tables* (Refer to ANSYS help for more information).

In addition, the velocity of the border between the fluid and the structure can be calculated by differentiating its corresponding displacement value. Then these values are given to the software as *Tables*. The validity of these values can be checked by using the menus of the software.

As the fluid is regarded viscous, no-slip boundary condition is considered for the blade surface.

The final output of this section is the pressure distribution of the blade surface which is sufficient for computing the aerodynamic forces and moments. Fourier transformation is utilized for obtaining the real and the imaginary components of these forces during one cycle.

2.5. Parametric Substitution of the Aerodynamic Forces in Dimensionless Equation Set

As the aerodynamic effects on structures are often expressed as pressure or force coefficients, it is better to non-dimensionalize the other quantities of the equations for uniqueness. After the required conversions, the generalized aeroelastic equations are rewritten as

$$\begin{bmatrix} 1 & -\bar{B}x \\ -\bar{B}x & \mathrm{r}_\theta^2 \end{bmatrix}\begin{bmatrix} \frac{\ddot{q}_h}{b} \\ \ddot{q}_\theta \end{bmatrix}+\begin{bmatrix} 2\zeta_{hs}k_h & 0 \\ 0 & 2\mathrm{r}_\theta^2\zeta_{\theta s}k_h \end{bmatrix}\begin{bmatrix} \frac{\dot{q}_h}{b} \\ \dot{q}_\theta \end{bmatrix}+\begin{bmatrix} k_h^2 & 0 \\ 0 & \mathrm{r}_\theta^2 k_\theta^2 \end{bmatrix}\begin{bmatrix} \frac{q_h}{b} \\ q_\theta \end{bmatrix}=\frac{1}{\pi\mu}\begin{Bmatrix} \frac{C_{FG}}{b} \\ \frac{C_{MG}}{b^2} \end{Bmatrix} \tag{8}$$

For this purpose the two sides of the first relationship has been multiplied by b/U_∞^2 and the second relation by $1/U_\infty^2$.

3. Aerodynamic Forces Generalization Method

In the current research, aeroelastic analysis is performed by loosely coupled method. At first, the aerodynamic forces are written as a function of reduced frequency, mode shape and the resulting matrices.

If these forces are considered constant along the span (Otherwise piecewise integration must be used), the final formula for obtaining the generalized aerodynamic forces is

$$\begin{Bmatrix} \frac{C_{FG}}{b} \\ \frac{C_{MG}}{b^2} \end{Bmatrix}=\int_0^l \left\{ C(p)\begin{bmatrix} \phi & 0 \\ 0 & \theta \end{bmatrix}\begin{bmatrix} \phi & \theta \\ \phi & \theta \end{bmatrix}\begin{Bmatrix} \frac{q_h}{b} \\ q_\theta \end{Bmatrix}\right\}\frac{dy}{l}$$

$$C(p)=\begin{bmatrix} C_{Fh}(p) & \frac{C_{F\theta}(p)}{b} \\ \frac{C_{Mh}(p)}{b} & \frac{C_{M\theta}(p)}{b^2} \end{bmatrix}. \tag{9}$$

The bending and torsional natural frequencies are then orthonormalized by the following relation.

$$\int_0^l \phi_i^2\frac{dy}{l}=1-\int_0^l r_h^2\psi_i^2\frac{dy}{l}=1-\psi_{norm}$$

$$\int_0^1 \theta_i^2\frac{dy}{l}=1 \tag{10.a}$$

By this approach, the terms are simplified to this result

$$\begin{Bmatrix} \frac{C_{FG}}{b} \\ \frac{C_{MG}}{b^2} \end{Bmatrix} = C(p) \begin{bmatrix} 1-\psi_{norm} & \bar{B} \\ \bar{B} & 1 \end{bmatrix} \begin{Bmatrix} \frac{q_h}{b} \\ q_\theta \end{Bmatrix} \quad (10.b)$$

4. Establishing Aeroelastic Equation

In the previous section, a parametric relation was for computation of the generalized aerodynamic forces as a function of $C(p)$ which is a representative of the aerodynamic forces, thus it is necessary to calculate $C(p)$ by using the existing aerodynamic data. In this method, aerodynamic forces are represented as a function of reduced frequency by Roger' approximation technique in laplace domain.

$$C(p) = C_1 + C_2 p + C_3 p^2 + \sum_{m=4}^{M} \frac{C_m p}{p + \beta_{m-2}} \quad (11)$$

Where C_1 , C_2 and C_3 represent quasi-elastic, quasi-damping and quasi-inertia coefficients. p Is a laplace variable. Also, in order to have more accurate answers, an augmented variable is defined as $q_m = (p/(p+\beta_{m-2}))q$, so this approach can also facilitate aeroservoelasticity analysis of turbomachinery blades.

The aerodynamic coefficients are then calculated at several reduced frequencies by the aerodynamic method described in this paper, and then Roger's approximation technique is used by applying the method introdued by Karadal et al (2007). By applying the approximated generalized forces in eq.8, the final aeroelastic equation is transferred to the laplace form. i.e.

$$(M_s p^2 + C_s p + K_s)q = RHS$$

$$RHS = (A_e C_1 + A_e C_2 p + A_e C_3 p^2 + A_e \sum_{m=4}^{M} \frac{C_m p}{p+\beta_{m-2}})q$$

$$M_s = \begin{bmatrix} 1 & -\bar{B}\bar{x} \\ -\bar{B}\bar{x} & r_\theta^2 \end{bmatrix},$$

$$C_s = \begin{bmatrix} 2\varsigma_{hs} k_h & 0 \\ 0 & 2\varsigma_{\theta s} r_\theta^2 k_\theta \end{bmatrix} \quad (12)$$

$$K_s = \begin{bmatrix} k_h^2 & 0 \\ 0 & r_\theta^2 k_\theta^2 \end{bmatrix}, \; q = \begin{Bmatrix} \frac{q_h}{b} \\ q_\theta \end{Bmatrix},$$

$$A_e = \frac{1}{\pi\mu} \begin{bmatrix} 1-\psi_{norm} & \bar{B} \\ \bar{B} & 1 \end{bmatrix}$$

As this aeroelastic equation is non-linear, it must be solved by state space approach. So its inverse laplace transformation leads to

$$M\ddot{q} + B\dot{q} + Kq = \sum_{m=3}^{M} A_e C_m q_m, \; M = M_s - A_e C_2$$
$$B = C_s - A_e C_1 , \; K = K_s - A_e C_0 \quad (13)$$

In this research, the solution of the eigenvalue equation by state space method is accomplished for $M = 6$.

To find the flutter speed, the inlet fluid velocity and thus k_h and k_θ are varied until the real part of one of the eigenvalues becomes zero. The effects of either k_h or k_θ can be observed in eq.8. The real part of the eigenvalue represents the damping ratio and the imaginary part represents the damping frequency. The flutter is occurred once $\mu \geq 0$.

Furthermore, for simulation of the dynamic behavior of the system, the eigenvector must also be derived. For each eigenvalue, the equation

$$(\underline{\underline{A}} - p\underline{\underline{I}})\underline{x} = \underline{0} \quad (14)$$

can be solved for its corresponding eigenvector. so the time evolution of the structure is obtained by this formula.

$$x(t) = (\underline{\underline{X}} e^{\Lambda t} \underline{\underline{X}}^{-1})x(0) \quad (15)$$

Thus, the motion of the generalized coordinate can be evaluated versus time. It is obvious that by having the mode shapes of bending and torsion described in the previous sections, and multiplying those by components q_h/b and q_θ , the equation of motion in each section of the blade can be obtained.

5. Aeroelastic Analysis by Conventional Method

In this approach that sometime is referred to as double scanning method, the frequencies are non-dimensionalized with respect to the tosional natural frequencies. The earoelastic quantities of this method are non-dimensionalized by dividing eq. 4 by ω_θ^2 .

$$M_s = \begin{bmatrix} 1 & -\bar{B}\bar{x} \\ -\bar{B}\bar{x} & r_\theta^2 \end{bmatrix}, \; C_s = \begin{bmatrix} 2\zeta_s(\frac{\omega_h}{\omega_\theta}) & 0 \\ 0 & 2r_\theta^2 \zeta_s \end{bmatrix}$$

$$K_s = \begin{bmatrix} (\frac{\omega_h}{\omega_\theta})^2 & 0 \\ 0 & r_\theta^2 \end{bmatrix}, \; X^T = \begin{bmatrix} \frac{q_h}{b} & q_\theta \end{bmatrix} \; F_G^T = \begin{bmatrix} \frac{C_{FG}}{b} & \frac{C_{MG}}{b^2} \end{bmatrix},$$

$$A_e = \frac{(\frac{\omega_h}{\omega_\theta})^2}{\pi\mu k_h^2}$$

$$M = M_s \ , \quad B = C_s - A_{ei} C_{GI} \ , \quad A_{ei} = \frac{(\omega_h / \omega_\theta)}{\pi \mu k_h k}$$

$$K = K_s - A_{er} C_{GR} \ , \quad A_{er} = \frac{(\omega_h / \omega_\theta)^2}{\pi \mu k_h^2}$$

After substitution, this general relationship is achieved.

$$M \ddot{X} + B \dot{X} + K X = 0 \tag{16}$$

According to this method, the flutter speed can be achieved by trial of various k values for a constant mass ratio.

6. Claculations and Discussions

A tuned bladed disk system of a gas turbine compressor made of tenth standard configuration airfoil is subjected to an upstream air flow. The flutter velocity and the relevant equation of motion are desired. Also, the difference of aeroelastic behavior between two blades with cambered and uncambered airfoil but with equal area will be discussed. In tenth standard configuration, the thickness distribution is represented by this equation.

$$T(x) = H_T (2.969x^{0.5} - 1.26x - 3.516x^2 + 2.843x^3 - 1.036x^4) \quad 0 \le x \le 1 \tag{17}$$

Where H_T is the nominal blade thickness. The camber distribution is given by

$$C(x) = H_C - R + \sqrt{\left\{R^2 - (x - 0.5)^2\right\}} \ 0 \le x \le 1 \tag{18}$$

Where H_C (>0) denotes the height of the camber-line at midchord and R is the radius of the circular arc camber line and equals

$$R = \frac{\left\{H_C^2 + 0.25\right\}}{2H_C} \tag{19}$$

In this aeroelastic case, the structure characteristics are given as follows;

l=span=0.12 m	blade spa
$\rho_s = 4460\ kg/m^3$	density of the structure
E=114 G Pa	module of elasticity
υ=0.31	Poisson's ratio
$\gamma = 1.7556$	shear coefficient
G = 4.3511e10	shear modulus
$H_T = 0.06$, $H_C = 0.05$	in cambered airfoil
$\forall x : C(x) = 0$	in uncambered airfoil
$\varsigma_h = 0.0015$	Damping ratio of bending and torsion
$\varsigma_t = 0.0015$	

The characteristics of this cambered airfoil are equivalent to NACA0006 airfoil.

Natural frequency calculation

In order to determine the area and the moment of inertia, a program named *ROSANE* was provided in MATLAB and the data pertaining to the thickness distribution and the camber of airfoil was given to it.

Uncambered Airfoil

A = 4.0815e-004 the airfoil area

$x_{center} = 0.0418$ Mass center position

$z_{center} = 0$

Determination of the elastic center (shear center): By taking $C(x) = 0$ for every x in eq.18, one can conclude that

$$x_a = x_{center} \qquad y_a = y_{center}$$

The elastic center is moved towards x axis to the decoupling point at which the z coordinate is the same as the center. The coordinate of the decoupling point is

$$x_o = x_{center} \qquad z_o = z_{elastic\ point}$$

Moments of inertia of the airfoil surface with respect to the decoupling point is

Ix_elastic = Ixo=8.4661e-10

r_torsion = 0.0233 with respect to the elastic center

r_h = 0.0014 (with respect to the x axis)

The ratio of the radius of gyration to the span (non-dimensional radius of gyration) is

$$k = \frac{\sqrt{I_{xo} / A_s}}{l} = 0.0120$$

Cambered Airfoil

For cambered airfoil, the previously stated quantities are

A = 4.1013e-004

x_centr = 0.0418

z_centr = 0.0038

Ix_elastic = 2.0643e-9

r_h = 0.0022

r_t = 0.0249

$k = 0.0187$

The airfoil area is approximately the same in both cases. However, the moments of inertia due to the increment of the airfoil camber are greatly changed.

A code named *Rezone* was provided based on the equation set provided by Kardal et al (2007) which was solved by numerical approach; thereby solution of these equations yields wave numbers. Hence, a, b and ω_n can be obtained as a function of the radius of gyration.

In the post processing step of this code, the natural frequencies can be plotted with respect to the radius of gyration in the case of cambered and uncambered airfoil. Fig.3 shows typically the variation of natural frequency with respect to non-dimensional radius of gyration.

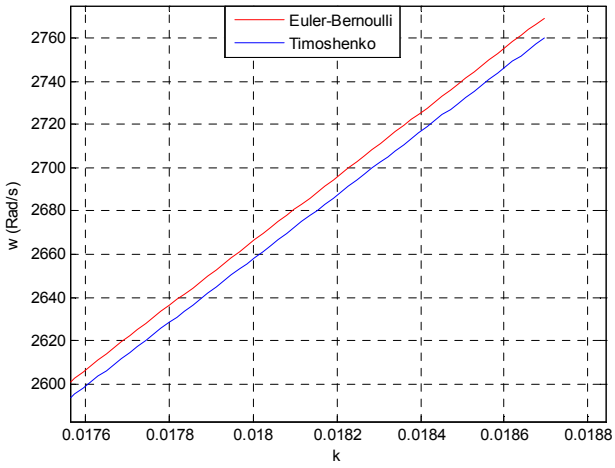

Figure 3. *The first natural frequencies of Euler-Bernoulli and Timoshenko beam models for the specified cambered airfoil based on gas as fluid.*

In addition, the first wave numbers and natural frequencies are listed Table 3 and Table 4. The difference of these two cases indicates the great effect of camber on natural frequency.

Table 1. *Wave number and natural frequencies of the blade with uncambered airfoil.*

Wave numbers of Timoshenko model		$\omega_{s1}(rad/s)$	
a	*B*	Timoshenko	Euler- Bernoulli
1.8747	1.8728	1773.4934	1775.9100

Table 2. *Wave numbers and natural frequencies of the blade with cambered airfoil.*

Wave numbers of Timoshenko model		$\omega_s(rad/s)$	
a	*B*	Timoshenko	Euler- Bernoulli
1.8742	1.8696	2757.2796	2766.3820

For verification of the frequencies resulting from *Rezone* code, the natural frequency of cambered airfoil obtained by this code was compared with the result obtained by ANSYS. The output of *Rezone* was consistent with what achieved by ANSYS. The procedure to analyze the structural model by ANSYS was as follows; Element BEAM44 was used for modeling Timoshenko beam. Concerning the capabilities of this element, the value of Poisson' ratio was given to this program so that the shear deformation can be considered. Furthermore, in order to take the rotary inertia into account, a rectangular section whose area equals the airfoil area was generated and then meshed with fine grids.

In Euler-Bernoulli beams, element BEAM54 is used and the Poisson's ratio was considered zero so that the effects of rotary inertia and shear deformation were ignored. The results were

$\omega_{ls} = 2759.6826\ Rad/s$ Timoshenko model

$\omega_{ls} = 2766.7184\ Rad/s$ Euler-Bernoulli model

Which agree with the Rezone output. Moreover, the torsional natural frequency of the blade was achieved by eq.7 which results

$\omega_{ts} = 40885.8454$ rad/s.

In order to verify the results of torsional natural frequency, the modal analysis of the blade was performed by ANSYS. In this model, the length of the blade was subdivided by 100 nodes. Then elements COMBINE14 which have stiffness was placed between each two nodes and elements MASS21 which consist of moment of inertia were defined for each node (except the node placed on the root of the blade).

Note that the distance between the first node and the blade root and so the moment of inertia is half of the other intervals, so the stiffness of this element is two times of the other. By this procedure the following first natural frequency was obtained for torsional frequency.

$$\omega_{ts} = 41292.7011 \text{ rad/s}$$

Which was consistent with the previously calculated result.

7. Calculation of the Aerodynamic Forces by Applying the Program Provided by ANSYS

As the bladed disk system (Blisk) was assumed to be tuned, the analysis was simplified to a single blade and its surrounding aerodynamic spaces. To determine the aerodynamic forces, the characteristics of the airfoil specified so far was entered to the code named *Vazan* that was written in ANSYS/FLOTRAN. This code was executed at several reduced frequencies. In this step, the condition of the problem solution was determined and the fluid was introduced to *Vazan* as gas, then some appropriate commands were issued so that the properties can be varied as a function of temperature and pressure. However, as predicted, it was observed in this report that the variation of density and viscosity was negligible. As in many other references, the initial conditions and the inlet properties of the fluid were considered 10° angle of attack, 0.7 inlet Mach number and standard condition.

The Reynolds number may exceeds the laminar flow threshold, because flutter may takes place in a free stream velocity which is in transonic or supersonic condition, although the fluid enters the blade path in a low angle of attack, so the turbulence of the flow was also introduced to the program. There are various models of turbulence in ANSYS such as $k-\varepsilon$, $k-\omega$ and combination of them. Some tests were accomplished, and it was observed that $k-\varepsilon$ model is the most adequate.

The solution of the problem is also done in time steps, thus the output of this code is pressure distribution in each time step, and the force (lift) and the aerodynamic moment coefficient of the entire model was computed at every time step of the cycle by using the pressure distribution obtained from the previous step. The real and imaginary components of the lift and aerodynamic moment coefficients were obtained by Fourier transformation, in both of cambered and uncambered airfoil cases. The results are demonstrated in Tables 3 to 6.

Table 3. *The values of forces and moments applied on the uncambered airfoil in bending oscillation.*

Reduced frequency	Lift coefficient	Moment coefficient
0.25	0.17765 -0.11783i	-9.8707E-04+3.3168E-03i
0.50	0.72614 -0.31617i	-2.2700E-03 +8.3711E-03i
0.75	1.6327 -0.63079i	-1.0045E-03 +1.2667E-02i
1.00	2.9793 -1.1387i	1.5441E-03 +1.6922E-02i
1.25	5.0791 -1.8442i	6.3903E-03 +2.1186E-02i
1.50	7.3461 -2.5477i	1.3635E-02 +2.3231E-02i

Table 4. *The values of forces and moments applied on the uncambered airfoil in torsional oscillation.*

Reduced frequency	Lift coefficient	Moment coefficient
0.25	-4.1929E-03 -1.3187E-02i	1.9211E-04 -2.7123E-05i
0.5	-9.0745E-03 -2.6261E-02i	5.6821E-04 -1.8174E-04i
0.75	-1.4538E-02 -3.8987E-02i	1.0488E-03 -3.6724E-04i
1.0	-1.4391E-02 -5.6590E-02i	1.5671E-03 -5.0427E-04i
1.25	-1.2532E-02 -7.3824E-02i	2.3474E-03 -7.6659E-04i
1.5	-1.5819E-02 -8.4071E-02i	3.2021E-03 -9.8503E-04i

Table 5. *The values of the forces and moments applied on the cambered airfoil in bending oscillation.*

Reduced frequency	Lift coefficient	Moment coefficient
0.25	0.17124 -0.11408i	-6.1341E-04 +3.5263E-03i
0.50	0.71264 -0.31106i	-1.9681E-03 +8.8104E-03i
0.75	1.6100 -0.61952i	-8.2827E-04 +1.3378E-02i
1.00	2.9457-1.1341i	1.8875E-03 +1.7683E-02i
1.25	4.7458 -1.7184i	5.8285E-03 +2.0104E-02i
1.50	6.8503 -2.3670i	1.1751E-02 +2.2083E-02i

Table 6. *The values of forces and moments applied on the cambered airfoil in torsional oscillation.*

Reduced frequency	Lift coefficient	Moment coefficient
0.25	-3.2311E-03 -1.4350E-02i	1.9841E-04 -3.9452E-05i
0.50	-8.8571E-03 -2.6821E-02i	5.7089E-04 -2.1586E-04i
0.75	-1.6302E-02 -4.1274E-02i	1.0875E-03 -3.9875E-04i
1.00	-1.4495E-02 -6.2360E-02i	1.5640E-03 -4.8191E-04i
1.25	-8.8248E-03 -7.1010E-02i	2.1518E-03 -6.9381E-04i
1.50	-1.4690E-02 -7.7265E-02i	2.9653E-03 -8.8725E-04i

To verify the results, a typical real and imaginary chordwise pressure distribution at bending reduced frequency of 0.5 and Mach number of 0.7 and unit oscillation amplitude was calculated by *Vazan*. On the other hand, at the same condition, the pressure distribution was derived from spectrum code which was introduced by Lawrence et al (2000) and the lift and moment coefficient were calculated by geometrical methods which agreed with *Vazan*.

8. Investigating the Effects of Camber on Flutter Characteristics of Blades

This part is devoted to the computation of flutter speed and its corresponding frequency with the results of structural and aerodynamic analysis, and *the aeroelastic behavior of cambered airfoils with uncambered ones was performed by considering four characteristics: radius of gyration, variation of aerodynamic loading, torsion/bending coupling, and Timoshenko beam factors.*

For this task, the aeroelastic behavior of the blade with uncamberd airfoil was determined at first. After that, the above mentioned aspects were considered, and the corresponding aeroelastic equation was solved, and the normalized bending and torsional mode shapes of the structure were obtained. The aerodynamic loading terms were then substituted in the main aeroelastic equation as a function of reduced frequency. Afterwards, the final equation was solved by state space approach and utilizing augmented state vector, so that the eigenalues were obtained. The free stream velocity was then increased so that at a certain velocity the real component of the eigenvalue became zero. This velocity is termed flutter speed, and the imaginary part of the eigenvalue is the flutter frequency. This procedure was repeated for each case. The results of these computations are shown in the following Table 7. The second row of this table consists of the aeroelastic results via the effects of airfoil camber on aerodynamic loading, radius of gyration, and bending/torsion coupling. The third one indicates the effects of rotary inertia and shear deformation due to airfoil camber on flutter characteristics.

Table 7. *Flutter characteristics of the specified blade with cambered airfoil using steam and gas as fluid.*

Structural Model	Flutter Characteristics
Cambered Airfoil Using steam as fluid	$U_{flutter} = 163.09$ $\omega_{flutter} = 2650.756$
Cambered Airfoil Using gas as fluid	$U_{flutter} = 140.1095$ $\omega_{flutter} = 2682.0449$

Root locus plots of the eigenvalues in cambered airfoil with steam and gas as fluid are also demonstrated in Fig. 4 and fig. 5.

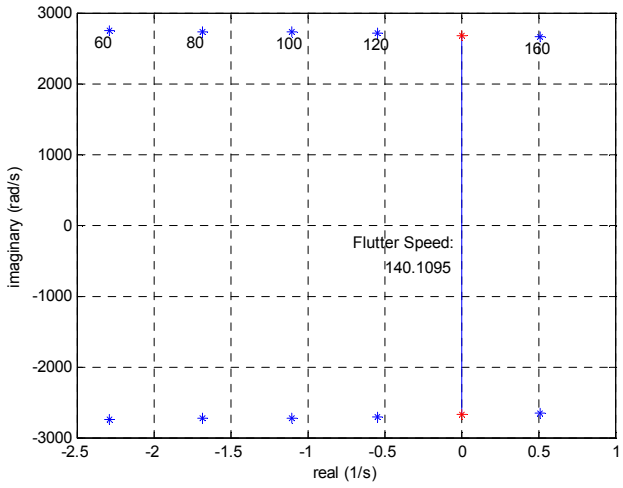

Figure 4. *Root locus plot of the eigenvalues of the specified blade with cambered airfoil and gas as fluid by the application of Timoshenko theory.*

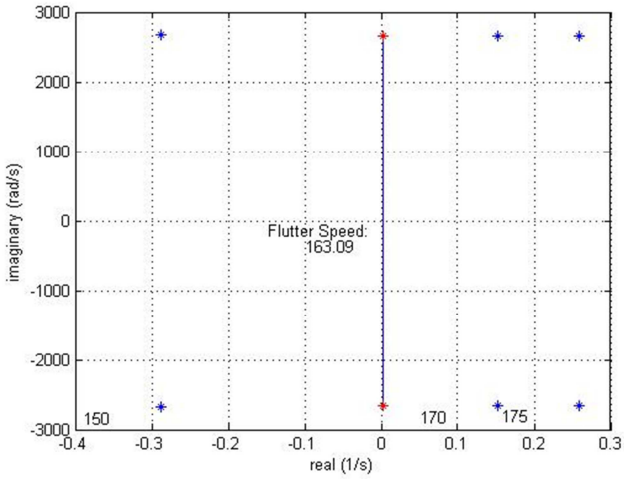

Figure 5. *Root locus plot of the eigenvalues of the specified blade with cambered airfoil and steam as fluid by the application of Timoshenko theory.*

In higher modes the flutter occurs at very high speed so that the free stream velocity does not have physical meaning. In addition, the flutter of the first mode is predominant, because the problems pertaining to flutter do not actually allow the speed to rise up to the higher modes. For example the second flutter characteristic of this typical case with cambered airfoil by Timoshenko theory is

$$V = 2876.1233\ m/s\ ,\ \omega = 16094.6144\ Rad/s\ .$$

8.1. Comparison of the Final Results with Conventional Method

For verifying the final results, the flutter equation in the first mode of Timoshenko model was rewritten based on eq.16, and the equation was solved by state space approach and by trying different values of k until an adequate value was determined at which the real part of the eigenvalue tends to zero.

The aerodynamic forces were calculated in two assumed condition and the resulting eigenvalues were obtained from eq.16. Interpolation of these reduced frequencies and their flutter speeds were then fed into Vazan code whose output is entered into the earoelastic equation 16. Next, the flutter speed was estimated by this relationship.

$$U_{flutter} = \frac{\omega_{New} b}{k} = \frac{2760.0091 \times 0.05}{0.9890} = 139.5353\, m/s$$

As the result shows, the flutter speed converges back to the value determined by Roger's approximation and the real part tends to zero at a moderately low rate. By continuing the iterations, more accurate results will be obtained. However, the above flutter velocity agrees the Roger's approximation solution which was achieved at the previous section.

8.2. Determining and Plotting the Equations of Motion

It was assumed that the start of excitation is at zero $(t = 0)$ of the time range considered. With the initial condition

$$q_h(t=0) = 1, \quad q_t(t=0) = 1.$$

The plunging and pitching displacements of the generalized coordinates of the blade are plotted versus time at the flutter as shown in Fig.6 and Fig. 7.

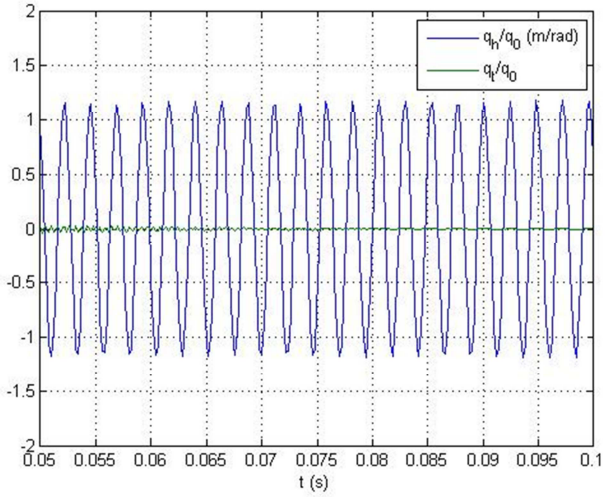

Figure 6. *Time simulation of Pitching/Plunging vibration of the blade with cambered airfoil and steam as fluid by Timoshenko beam theory at flutter* $(U_\infty = 163.09\ m/s)$, $(\omega = 2650.756$ Rad/s$)$.

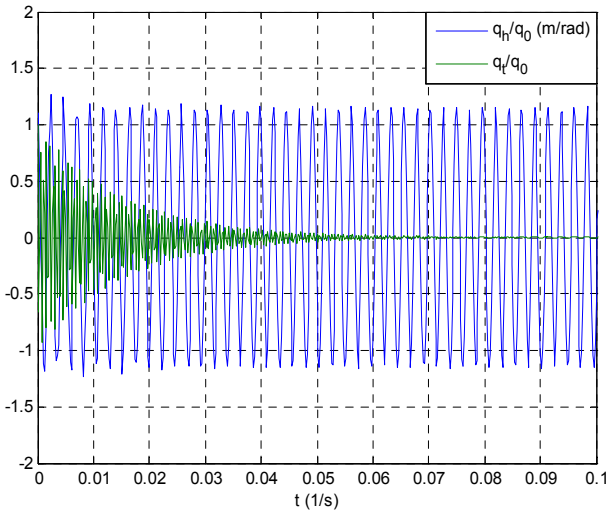

Figure 7. *Time simulation of Pitching/Plunging vibration of the blade with cambered airfoil and gas as fluid by Timoshenko beam theory at flutter* $(U_\infty = 140.1095 m/s)$, $(\omega = 2682.0449$ Rad/s$)$.

As shown in Fig.6 and Fig. 7, the plunging motions are predominant and the motions of the other degrees of freedom will cease after elapsing some cycles. Thus, the relations were simplified, and after simplifying the terms and multiplying them by the mode shapes, the following equations of motion were achieved;

The final equation of plunging motion of the blade having cambered airfoil by using Timoshenko theory is

$$h(y,t)=\phi(y)q_h(t)=[2.1131\sin(15.6208y)-2.8688\cos(15.6208y)-2.1027\sinh(15.5933y)+2.8688\cosh(15.5933y)]\times 1.1583\cos(2682.04t). \quad (20)$$

The final equation of pitching motion of the blade having cambered airfoil by using Timoshenko theory is

$$\theta(y,t)=\sqrt{16.6667}\sin(\frac{\pi}{0.24}y)\times 4.09\times 10^{-5}\cos(2682.04t). \quad (21)$$

9. Conclusion

In this research paper we calculate the flutter speed in turbine blade using steam and gas as fluid. Equation of motion in Timoshenko beam is obtained and by using steam and gas as fluid we compare the flutter speed in gas and steam turbine. The results show that:

1-. Elastic effects: Increment of the radius of gyration by giving camber to the midline of the airfoil led to the natural frequency increment, thereby rising flutter velocity (elastic effects).

2-. Dynamic effects: Airfoil camber increased rotary inertia and shear deformation, and bending/torsion coupling, thereby reducing flutter velocity, but had less effect than elastic factors.

3-. Generally, adequate camber of the airfoil makes flutter suppression besides increasing aerodynamic efficiency.

4-. By using steam as fluid we can delay the flutter speed.

References

[1] ANSYS Inc (2004). Release 11.0 Documentation for ANSYS.

[2] Baldelli DH, Lind RC, Brenner M (2005). Robust Aeroelastic Match-Point Solutions Using Describing Function Method. J. Aircraft. 42(6).

[3] Beer FP, Johnstone ERJ (1985), Mechanics of Materials. 2nd ed., McGRAW-HIL Book Company, pp 274-281.

[4] Boyce MP (2001), Gas Turbine Engineering Handbook, Gulf Professional Publishing, Houston, Texas

[5] Campobas MS (2004). Effects of Flow Instabilities on the Linear Harmonic Analysis of Unsteady Flow in Turbomachinery, PhD dissertation. University of Oxford, Oxford, England.

[6] Doi H, Alonso JJ (2002). Fluid/Structure Coupled Aeroelastic Computations for Transonic Flows in Turbomachinery, Proceedings of ASME Turbo Expo held at Amsterdam, The Netherlands, GT-30313.

[7] Feistauer M (2007). Finite Volume and Finite Element Methods in CFD (Numerical Simulation of Compressible Flow), Faculty of Mathematics and Physics, Charles University Prague.

[8] Fransson TH, Verdon JM (1992). Updated report on Standard Configuration for Unsteady Flow Through Vibrating Axial-Flow Turbomachine-Cascades, Standard Configurations, 6/21/01.

[9] Han JH, Han JH, Tani J, Qiu J (2006). Active Flutter Suppression of a Lifting Surface Using Piezoelectric Actuation and Modern Control Theory. J. Sound Vib. 291(3/5): 706-722.

[10] Han SM, Benaroya H, Wei T (1999). Dynamics of Transversely Vibrating Beams Using Four Engineering Theories. J. Sound Vib. 225(5): 935-988.

[11] Hodges DH, Pierce GA (2002). Introduction to Structural Dynamics and Aeroelasticity, Cambrides University Press.

[12] Karadal FM, Seber G, Sahin M, Nalbantoglu V, Yaman Y (2007). State Space Representation of Smart Structures under Unsteady Aerodynamic Loading, Ankara International Aerospace Conference held at Ankara, Turkey, AIAC-2007-034.

[13] Lawrence C, Spyropoulos E, Reddy TSR (2000). Unsteady Cascade Aerodynamic Response Using a Multiphysics Simulation Code, NASA/TM-209635.

[14] Lind R (2002). Match-Point Solutions for Robust Flutter Analysis. J. Aircraft. 39(1): 91-99.

[15] Liu F, Cai J, Zhu, Tsai HM, Wong ASF (2001). Calculation of Wing Flutter by a Coupled Fluid-Structure Method. J. Aircraft. 38(2): 332-4.

[16] Pototzky AS (2008). Modeling State-Space Aeroelastic Systems Using a Simple Matrix Polynomial Approach for the Unsteady Aerodynamics, NASA Langley Research Center, Aeroelasticity Branch, RTO-AVT-154.

[17] Poursaeidi E, Aieneravaie M, Mohammadi MR (2008). Failure analysis of a second stage blade in a gas turbine engine. J. Eng. Failure Analysis. 15: pp 1111–1129.

[18] Reddy TSR, Srivestava R, and Mehmed O (2002). STROP2-LE: A Mistuned Aeroelastic Analysis System Based on a Two Dimensional Linearized Euler Solver, NASA Glenn Research Center, Technical Support Package for Analyzing Aeroelasticity in Turbomachinery, NASA Tech Briefs, LEW-17477-1, NASA/TM-211499.

[19] Reddy TSR, Srivestava R, Mehmed O (1999). Flutter and Force Response Analyses of Cascades Using Two-Dimensional Linearized Euler Solver, NASA Glenn Research Center, NASA/TM-1999-209633.

[20] Reddy TSR, Bakhle MA, Trudell JJ, Mehmed O, Stefko GL (2004). LINFLUX-AE: A Turbomachinery Aeroelastic Code Based on a 3–D Linearized Euler Solver, NASA/TM-212978.

[21] Sadeghi M, Liu F (2005). Coupled Fluid-Structure Simulation for Turbomachinery Blade Rows, 43rd AIAA Aerospace Sciences Meeting and Exhibit held at Reno, NV, AIAA 2005-0018.

[22] Sadeghi M, Lui F (2005). Computation of Cascade Flutter by Uncoupled and Coupled Methods, Int. J. Computational Fluid Dynamics. 19(8): pp 559-569.

[23] Sadeghi M, Lui F(2005). Computation of Cascade Flutter by Uncoupled and Coupled Methods, Int. J. Computational Fluid Dynamics. 19(8): pp 559-569.

[24] Simsek M, Kocaturk T (2007). Free vibration analysis of beams by using a third-order shear deformation theory, Sadhana (Printed in India). 32(3): pp 167–179.

[25] Thomson WT(1988). Theory of Vibration with Applications, 3rd ed., Prentice Hall, Englewood Cliffs, New Jersey 07632.

[26] Willcox KE (2000). Reduecd-Order aerodynamic Models for aeroelastic Control of Turbomachines, PhD dissertation, Massachusetts Inst. Tech., Cambridge, Massachusetts, USA.